Thermochromic Narrow Band Gap Phosphors for Multimodal Optical Thermometry: The Case of Y^3-Stabilized beta-BiO:Nd^3

AUTHOR(S):

Back, Michele; Xu, Jian; Ueda, Jumpei; Benedetti, Alvise; Tanabe, Setsuhisa

CITATION:

Back, Michele ...[et al]. Thermochromic Narrow Band Gap Phosphors for Multimodal Optical Thermometry: The Case of Y^3-Stabilized beta-BiO:Nd^3. Chemistry of Materials 2022, 34(18): 8198-8206

ISSUE DATE:

2022-09-27

URL:

http://hdl.handle.net/2433/278910

CHEMISTRY OF MATERIALS

pubs.acs.org/cm

Article

Thermochromic Narrow Band Gap Phosphors for Multimodal Optical Thermometry: The Case of Y^{3+}-Stabilized β-Bi_2O_3:Nd^{3+}

Michele Back,* Jian Xu, Jumpei Ueda, Alvise Benedetti, and Setsuhisa Tanabe*

Cite This: *Chem. Mater.* 2022, 34, 8198−8206

Read Online

ACCESS | Metrics & More | Article Recommendations | Supporting Information

ABSTRACT: The design and development of effective luminescent thermal sensors have been driving technological progress in many different fields ranging from catalysis to biology and microelectronics, to name a few. The ratiometric concept of using the ratio between two luminescent emissions of lanthanide-doped phosphors allows overcoming some limitations resulting from the single emission-based thermometers. A fundamental requirement for the development of effective luminescent thermometers relies on efficient luminescence output, which is not always accessible. Therefore, alternative methods to probe the temperature in a reliable and simple way are still a challenge. Despite the conventional limits of using narrow band gap materials as hosts for lanthanoid ions, a smart design allows for the development of unusual phosphors with appealing properties. By taking advantage of the narrow band gap of Bi_2O_3 polymorphs, here we demonstrate the potential of the tetragonal Y-stabilized β-Bi_2O_3:Y^{3+},Nd^{3+} system as a multimodal thermometer combining the conventional Boltzmann thermometry based on Nd^{3+} together with the thermochromism of the host. With the aim of testing this new concept, the temperature dependence of the reflectance spectra was investigated. Moreover, from the application point of view, the chromaticity variations of the material described by means of simple thermometric parameters such as the ratio a^*/b^* and the hue angle h_{ab} are demonstrated to be particularly promising and already implemented in software commonly used worldwide. The results suggest the potential of the strategy of combining narrow band gap semiconductors with lanthanoid ions to design reliable and multimodal thermal sensors, paving the way to a new family of thermochromic and luminescent thermal sensors.

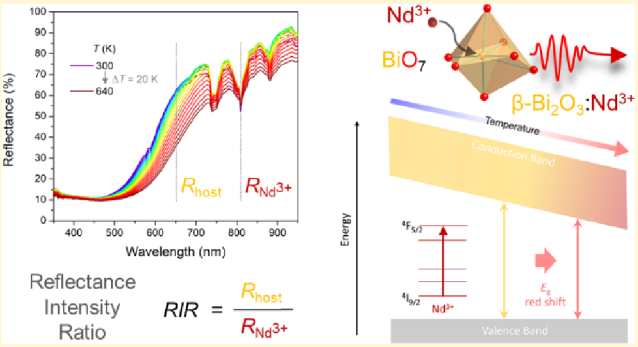

INTRODUCTION

Narrow spectral bands and long excited state lifetimes are two of the most relevant luminescence features of trivalent lanthanoid ions (Ln^{3+}) exploited to develop unique optical materials for applications ranging from lasers[1] to bioimaging,[2,3] from anti-counterfeiting[4] to temperature and pressure sensors,[5−7] to name a few.

The design of new Ln^{3+}-activated phosphors with advanced properties also relies on the interaction of the luminescent ions with the matrix. In fact, despite the variety of Ln^{3+}-activated insulator-based phosphors investigated and commercialized, new strategies to develop advanced phosphors implying unconventional materials are still a challenge. In this view, narrow band gap materials, conventionally avoided due to undesired interactions between their electronic band structure and the energy levels of the luminescent centers, have been recently demonstrated to be interesting matrixes for luminescent Ln^{3+} ions, paving the way to new opportunities.[8,9]

Among the potential narrow band gap hosts suitable to accommodate luminescent Ln^{3+} ions, bismuth oxide-based compounds are characterized by narrow band gap energies usually exploited in technological fields such as photocatalysis,[10,11] electronic and energy applications,[12,13] ferroelectrics,[12,14] scintillators,[15] topological insulators,[16,17] UV-filters,[18,19] and multiferroics.[13,20] Recently, the narrow band gap of Bi_2O_3 polymorphs (in the range of 1.5−3.8 eV depending on the polymorphs) was used to selectively tune the luminescent properties of upconverting (UC) lanthanide couples Bi_2O_3:Yb^{3+},Ln^{3+} (Ln = Er, Tm, and Ho) showing the possibility to get a single UC visible or NIR-to-NIR emission line.[8,9] The same strategy was also used to selectively achieve a single red emission in the case of $BiVO_4$:Yb^{3+},Tm^{3+}.[21] Moreover, it is worth noting that, theoretically, bismuth-based materials are particularly appealing hosts for effective phosphors due to their high refractive indexes, which directly influences the spontaneous emission probability of the luminescent centers.

Received: April 26, 2022
Revised: August 28, 2022
Published: September 12, 2022

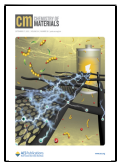

https://doi.org/10.1021/acs.chemmater.2c01262
Chem. Mater. 2022, 34, 8198−8206

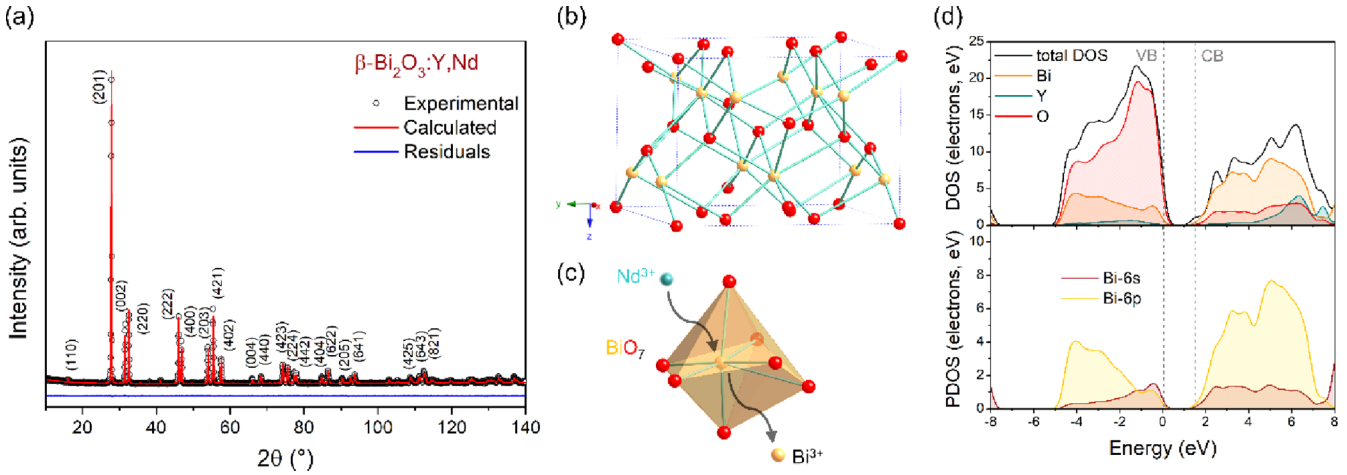

Figure 1. Crystalline and electronic structure of the tetragonal β-Bi_2O_3:Y^{3+},Nd^{3+} polymorph. (a) XRPD pattern along with Rietveld refinement and difference profile. (b) Crystalline structure and (c) local site of substitution for Nd^{3+} in β-Bi_2O_3:Y^{3+},Nd^{3+}. (d) T-DOS and P-DOS projected onto each constituent element.

In recent years, luminescent thermometers were demonstrated to be particularly intriguing to locally probe the intracellular temperature,[22−24] heating effects in microelectronic devices,[25] and also the phase transition temperatures[26,27] and the temperature of catalytic reactions.[28−31] In the field of optical thermometry, by taking advantage of the change with temperature of luminescent parameters such as the emission position, the band shape broadening, the emission intensity, the excited state lifetime, and so forth, many different techniques were adopted as thermal sensors so far.[5] Among them, the ratiometric concept of using the ratio of two luminescent signals (known as LIR, luminescent intensity ratio technique) is nowadays recognized as a successful self-reference method to overcome the lack of reliability of the thermometry based on a single emission band. Interesting strategies based on energy transfer between two luminescent ions,[32,33] the involvement of charge transfer bands,[34] or based on the use of excited state absorption[35,36] have been proposed. However, when two excited states from the same ion are thermally coupled by following the Boltzmann-distribution, the thermometers were demonstrated to be particularly reliable allowing precise temperature sensing,[37−41] with predictable behavior.

An intrinsic limit of all these techniques is the necessity of effective luminescence. In fact, strong luminescence leads to high signal-to-noise ratio, a necessary requirement for suitable thermal resolutions. Therefore, for many materials, the effectiveness of the thermometric performance is hampered by luminescence quenching.

Here, we introduce an alternative strategy to design multimodal thermometers based on thermochromic narrow band gap materials such as Bi_2O_3 doped with lanthanide ions. To achieve a high degree of reliability, the ratiometric concept is considered to describe different thermometric parameters. The β-Bi_2O_3:Y^{3+},Nd^{3+} system is proposed as a prototype to be used as a multimodal thermal sensor exploiting not only the luminescent properties of the lanthanoid ion (Nd^{3+}) but also the relative properties of its absorptions with respect to that of the host by means of in situ reflectance spectra acquired through a simple setup. Moreover, taking advantage of the narrow band gap energy of the host, colorimetric parameters are discussed and proposed as potential thermometric parameters with the advantage of easy availability in common software daily used.

RESULTS AND DISCUSSION

Nd^{3+}-Doped Narrow Band gap Y-Stabilized Tetragonal β-Bi_2O_3: Structural and Optical Properties. Bismuth oxide exists in six different polymorphs: (i) the room temperature-stable monoclinic α-phase, (ii) the tetragonal β-phase, the face-centered cubic δ-phase, the body-centered cubic γ-phase, the orthorhombic ε-phase, and the triclinic ω-phase.[42−44] By doping with suitable elements, it is possible to selectively stabilize some of the Bi_2O_3 polymorphs. In particular, by doping with different amounts of trivalent rare-earth ions (*e.g.*, Y^{3+}, Er^{3+}, La^{3+} *etc.*), the β- or δ-phase can be stabilized at room temperature.[42,43]

Figure 1a shows the X-ray powder diffraction (XRPD) patterns of the $(Bi_{0.945}Y_{0.05}Nd_{0.005})_2O_3$ system (labeled as β-Bi_2O_3:Y^{3+},Nd^{3+}) along with the Rietveld refinement, confirming the stabilization of the pure β-phase. The cell parameters and the results of the Rietveld refinement are shown in Table S1. The tetragonal β-Bi_2O_3 structure (space group $P4_2/nmc$) is characterized by a single site (8*g*) for Bi^{3+} and the stabilizer Y^{3+}, which proved to be particularly interesting when the single site is substituted with luminescent ions such as trivalent lanthanides Ln^{3+}. Indeed, the presence of a single substituting site for the Ln^{3+} ions (in this case Nd^{3+}) allows simplifying the interpretation of the results, thereby avoiding the misleading analyses resulting from signals of multi-site compounds. In addition, the depicted structure in Figure 1b and c evidences the low symmetry site (point group C_s) for Nd^{3+}.

To elucidate the origin of the top of the valence band (VB) and the bottom of the (CB), we conducted first-principles calculations using the CASTEP code. Focusing on the VB-top and CB-bottom, the partial density of state (P-DOS) and total density of state (T-DOS) of Y-stabilized β-Bi_2O_3 are plotted between −8 and 8 eV (Figure 1d). The top of the VB is mainly composed of O 2p orbitals, with a contribution of the Bi 6s and 6p orbitals, while the CB-bottom is mainly constituted by Bi orbitals. The analysis of the P-DOS of Bi evidences the overlap between Bi 6s and 6p orbitals at the top of the VB, a characteristic feature of the post-transition lone-pair metal

https://doi.org/10.1021/acs.chemmater.2c01262
Chem. Mater. 2022, 34, 8198−8206

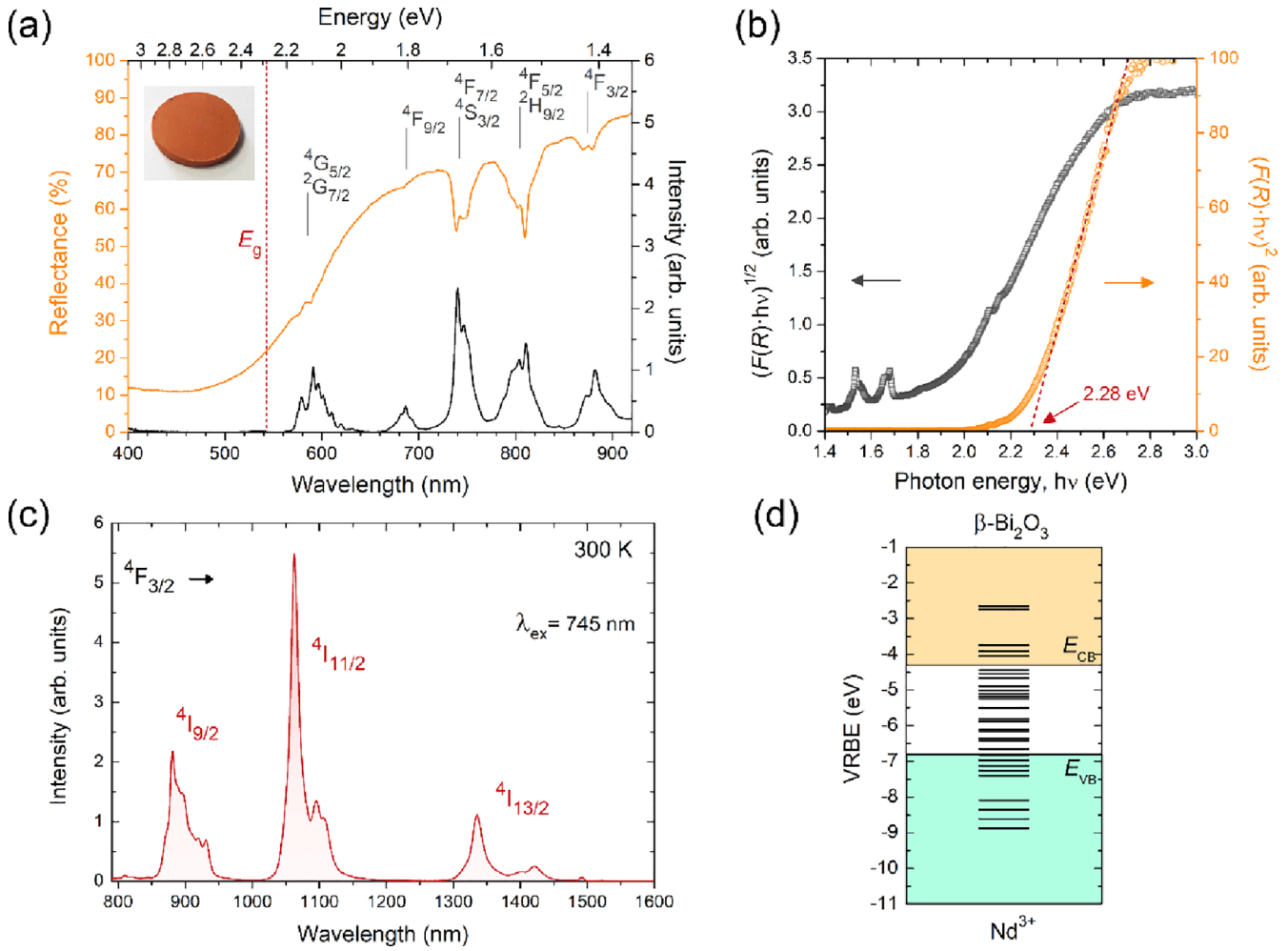

Figure 2. Electronic structure and optical properties of the narrow band gap β-Bi_2O_3:Y^{3+},Nd^{3+}. (a) Reflectance and PLE spectra collecting at 1060 nm along with the picture of the sample. (b) Tauc plot of the Kubelka–Munk function $F(R)$ for the estimation of the band gap energy. (c) Room temperature PL spectrum by exciting at 745 nm. (d) VRBE diagram for Nd^{3+} in β-Bi_2O_3:Y^{3+},Nd^{3+}.

compounds that can be considered as a fingerprint of the lone-pair asymmetric electron density.[45,46]

From the electronic structure point of view, bismuth oxide-based materials display narrow band gap energies that, from the one hand, can be detrimental for luminescent centers but, from the other hand, can be exploited to control the output emissions.[8,9] The picture of the pellet of the β-Bi_2O_3:Y^{3+},Nd^{3+} sample in Figure 2a clearly evidences the narrow band gap nature of the material. The reflectance spectra of the Nd^{3+}-activated system (Figure 2a) show the typical f–f transitions of Nd^{3+} along with the edge of the band-to-band absorption of the host.

The optical band gap energy of the material was estimated by the Tauc plot[47] of the Kubelka–Munk function[48] $F(R) = (1 - R)^2/2R$ from the diffuse reflectance (R). Figure 2b shows the Tauc plot of the Kubelka–Munk function for both the cases of direct and indirect semiconductors from which the direct band gap nature of the material is clearly confirmed, in agreement with the literature.[49,50] By extrapolating the intercept of the fitted straight line at $F(R) = 0$ of the $(F(R)\bullet h\nu)^2$ versus the $h\nu$ energy plot, a band gap energy E_g of 2.28 eV is estimated.

Together with the reflectance spectrum, Figure 2a compares the specular photoluminescence excitation (PLE) spectrum of Nd^{3+} collecting at 1060 nm. Even though the same f–f absorption peaks are characterized by the same position, the relative intensity is clearly different with a maximum excitation obtained by exciting through the $^4F_{7/2}/^4S_{3/2}$ excited state at about 745 nm. Moreover, at wavelengths lower than 560 nm no excitation bands are detected, in correspondence with the energy gap of the host.

Figure 2c shows the photoluminescence (PL) spectrum of β-Bi_2O_3:Y^{3+},Nd^{3+} by exciting at 745 nm, characterized by the typical emissions due to the $^4F_{3/2} \rightarrow {}^4I_{9/2}$ (~900 nm), $^4F_{3/2} \rightarrow {}^4I_{11/2}$ (~1060 nm), and $^4F_{3/2} \rightarrow {}^4I_{13/2}$ (~1350 nm) transitions. The decay curve of the PL collected at 1060 nm can be fitted by a single exponential (Figure S1) showing an $^4F_{3/2}$ excited state lifetime of 80 μs. Such a short lifetime for Nd^{3+} can be understood by considering the high refractive index of bismuth-based compounds.

Lanthanide-doped luminescent materials are conventionally designed by substituting the luminescent ions into suitable sites of insulators (wide band gap materials). In the case of narrow band gap materials used as hosts, their electronic structure can influence the optical processes from the energy levels of luminescent centers giving rise to new opportunities. If from one hand, narrow band gap materials can strongly quench the luminescence of lanthanide ions due to the

https://doi.org/10.1021/acs.chemmater.2c01262
Chem. Mater. 2022, 34, 8198–8206

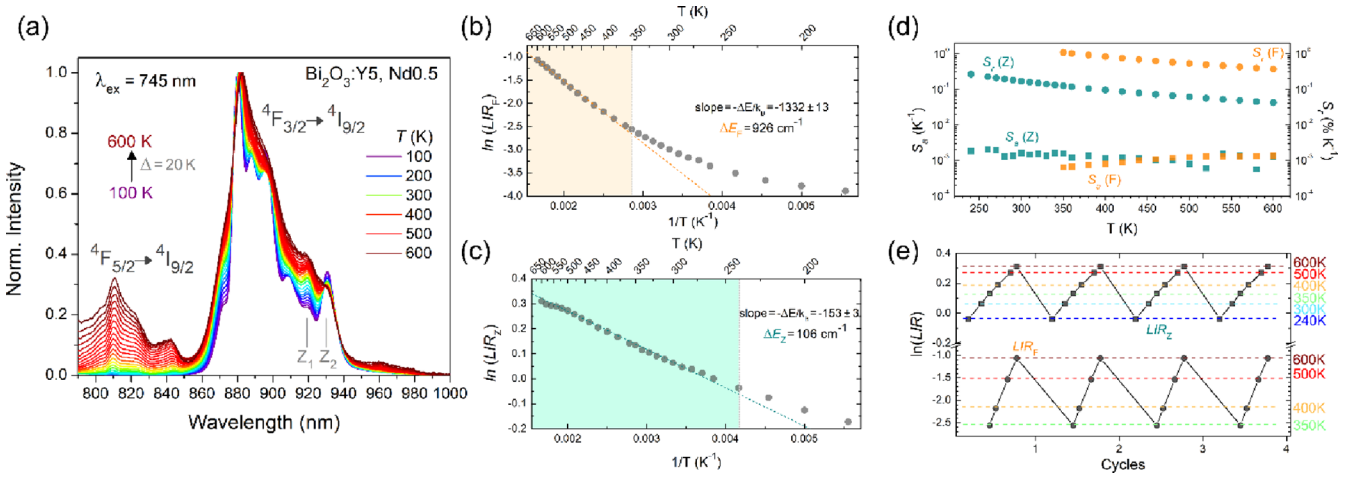

Figure 3. NIR-to-NIR Boltzmann thermometry. (a) Temperature dependence of the PL spectra in the 100−600 K range exciting at 745 nm spectra, normalized to the $^4F_{3/2} \rightarrow {}^4I_{9/2}$ emission. Boltzmann plot to calibrate the thermometers based on the ratio between $^4F_{3/2}$ and $^4F_{5/2}$ (b) and between the Kramers doublets Z-levels of $^4F_{3/2}$ (c) with the corresponding linear fits. (d) Temperature dependence of the absolute (S_a) and relative (S_r) sensitivities and (e) repeatability (R).

creation of non-radiative channels, on the other hand, the control of the relative position between the CB/VB of the host with respect to the energy levels of the luminescent centers can be used to design materials with new properties. For instance, by doping suitable (nano-)semiconductors characterized by direct band gaps with lanthanide ions, it is possible to take advantage of the large absorption cross section of the hosts to enhance the luminescence output from the f−f transitions. However, narrow band gap semiconducting materials that are not able to transfer electrons/holes to the luminescent ions can also be exploited to design smart materials in which this photons' blocking ability is a real technological advantage.

In the case of narrow band gap materials, the relative position of the top of the VB and the bottom of the CB of the host with respect to the luminescent ion energy levels should be known on an absolute scale in order to properly discuss the optical processes involved. In this view, the vacuum referred binding energy (VRBE) diagram introduced by Dorenbos for a wide variety of materials with respect to the lanthanoid ions[51] was demonstrated to be particularly suitable also for bismuth-based compounds.[52,53] By considering the flatband potential of −4.53 eV of β-Bi_2O_3[54] and the estimated optical band gap energy of 2.28 eV, the top of the VB can be fixed at E_V = −6.81 eV, while the exciton energy E^{EX} = 2.5 eV allows the CB-bottom at −4.31 eV to be fixed. Considering the average trend for the two polymorphs,[55] these values are consistent with the VRBE diagram reported for α-Bi_2O_3.[52] In addition, if we consider U(6,A) = 6.55,[52] the position of the energy levels of all the trivalent lanthanide ions can be fixed on the absolute scale, and the VRBE diagram of interest for Nd^{3+} in β-Bi_2O_3 is depicted in Figure 2d. The relative position of the energy levels of Nd^{3+} with respect to the top of the VB and the bottom of the CB shows how the excited states from which the luminescent transitions are originated (mainly $^4F_{3/2}$ and $^4F_{5/2}$) are quite far from the CB, excluding the possibility of a direct electron transfer from the excited state to the CB. Instead, the band gap energy estimated at about 2.28 eV well matched the lowest excited state detectable in the PLE spectrum, as evidenced by the vertical dashed line in Figure 2a, suggesting a direct effect of the host for photons with energy higher than its band gap.

Conventional NIR-to-NIR Nd^{3+}-based Ratiometric Luminescent Boltzmann Thermometry. To evaluate the potential of the system as a luminescent thermometer for different applications and investigate the fundamental phenomena involved, the effect of temperature on the PL spectra was investigated in the temperature range of 100−600 K.

In the field of luminescent thermometry, the use of Boltzmann-based thermometers allows a unique degree of reliability. By considering the potential use of Nd^{3+}-activated thermometers as bio-probes,[56−58] the excitation at 745 nm allows exploiting the first biological window in a NIR-to-NIR mode using the $^4F_{3/2}$-$^4F_{5/2}$ couple as a reliable Boltzmann-based thermometer. In fact, the conventional NIR-to-NIR thermometry, based on Nd^{3+}, is typically achieved by means of the 800 nm excitation ($^4I_{9/2} \rightarrow {}^4F_{5/2}/{}^2H_{9/2}$ transition) exploiting the Kramers doublets of $^4F_{3/2}$ induced by the crystal field splitting (conventionally labeled as Z_1 and Z_2) and characterized by a small energy gap with a consequent small value of relative sensitivity.[59,60]

Figure 3 summarizes the NIR-to-NIR thermometric performance of the β-Bi_2O_3:Y^{3+},Nd^{3+} system. The temperature dependence of the PL spectra in the first biological window is shown in Figure 3a evidencing the relative increase of the emission due to the $^4F_{5/2} \rightarrow {}^4I_{9/2}$ transition with respect to the $^4F_{3/2} \rightarrow {}^4I_{9/2}$ transition by increasing the temperature. The luminescence intensity ratio (LIR) between these two transitions can be used as a reliable thermal probe: $LIR_F = I_5/I_3$. I_5 and I_3 are the intensity emissions of the $^4F_{5/2} \rightarrow {}^4I_{9/2}$ and $^4F_{3/2} \rightarrow {}^4I_{9/2}$ transitions. The range of validity of the Boltzmann behavior and the energy gap ΔE_F between the $^4F_{5/2}$ and $^4F_{3/2}$ excited states can be estimated by plotting the logarithm of the LIR as a function of the inverse of the temperature $1/T$ (Figure 3b) and fitting the linear part through the general Boltzmann law:

$$LIR_{21} = \frac{I_2}{I_1} = A \exp\left(-\frac{\Delta E_{21}}{k_B T}\right)$$

where 2 and 1 refer to the general higher and lower excited states of the couple in thermal equilibrium, respectively. The

https://doi.org/10.1021/acs.chemmater.2c01262
Chem. Mater. 2022, 34, 8198−8206

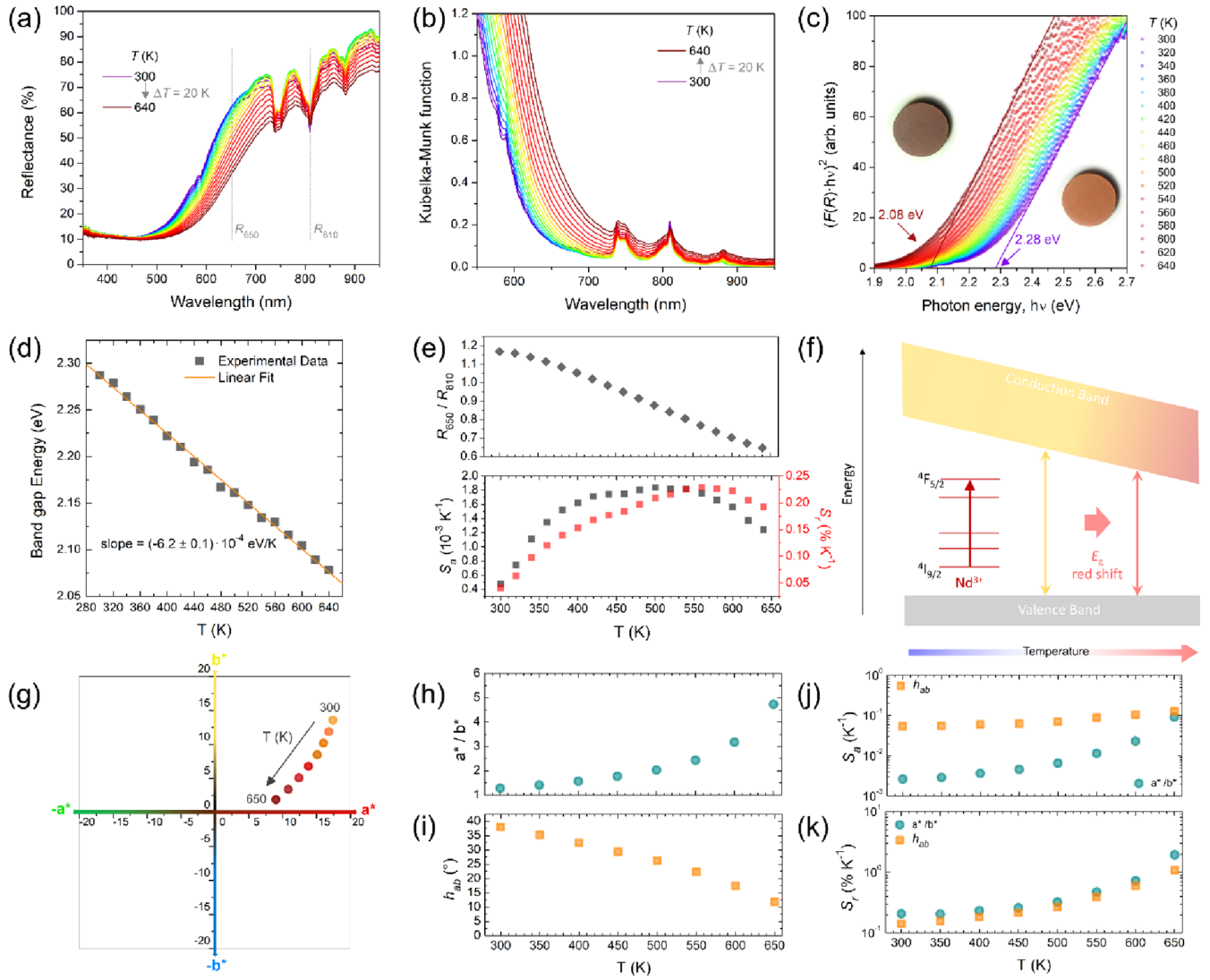

Figure 4. New thermometric parameters based on the temperature dependence of the reflectance spectra and colorimetric parameters. Temperature dependence of (a) reflectance spectra (the vertical dashed lines represent the reflectance values used for the RIR parameter), (b) Kubelka−Munk function and (c) Tauc plot for the estimation of the optical band gap energy. (d) Temperature dependence of the band gap energy with the linear fit. (e) Reflectance intensity ratio (RIR) used as the thermal parameter along with the absolute (S_a) and relative (S_r) sensitivities and (f) sketch of the thermometric parameter introduced based on the narrow band gap and the Nd^{3+} f−f transitions. (g) Thermochromic variation based on the colorimetric parameters a^* and b^* as a function of the temperature in the a^*b^* space, (h) thermometric parameter a^*/b^*, (i) hue angle h_{ab}, and relative thermometric parameter values (j) S_a and (k) S_r.

thermometer follows the Boltzmann law in the 350−600 K range, and the value of $\Delta E_F = 926 \pm 9$ cm^{-1}, estimated from the fit, is in good agreement with the value obtained from the spectra (~930 cm^{-1}). Instead, by considering the ratio between the emissions from the two Kramers doublets of $^4F_{3/2}$ (Z_1 and Z_2) to the higher-lying Stark level of $^4I_{9/2}$ ($LIR_Z = I_{Z_2}/I_{Z_1}$), a good linearity of the plot is obtained from 240 to 600 K (Figure 3c), and a $\Delta E_Z = 106 \pm 2$ cm^{-1}, obtained from the fit, is in good agreement with the value estimated from the spectra (~120 cm^{-1}).

The thermometric performance of these conventional Boltzmann thermometers can be evaluated by considering the absolute (S_a) and the relative sensitivities (S_r), defined respectively as

$$S_a = \left|\frac{\partial Q}{\partial T}\right|$$

$$S_r = \left|\frac{1}{Q}\frac{\partial Q}{\partial T}\right|$$

where Q is the thermometric parameter (in this case LIR_F and LIR_Z).

Figure 3d,e summarizes the thermometric performance for both the thermometric parameters. Being directly proportional to the energy gap between the two thermally coupled excited states ΔE_{21}, the values of S_r of the thermometer that uses the $^4F_{5/2}$ and $^4F_{3/2}$ states are higher than the one based on the Kramers doublets. Moreover, the values of S_r and S_a at 300 K agree with the general values of the Nd^{3+}-based Boltzmann thermometers based on the Kramers doublets reported in the literature (summarized in the Supporting Information, Table S2 and Figure S2).

Moreover, a thermal cycling experiment consisting in recording the thermometric parameters of four consecutive

https://doi.org/10.1021/acs.chemmater.2c01262
Chem. Mater. 2022, 34, 8198−8206

heating−cooling cycles was performed, and the repeatability (R) was estimated by the following relationship:

$$R\ (\%) = \left[1 - \frac{\max(|Q_m - Q_i|)}{Q_m}\right] \times 100$$

where Q_m is the mean thermometric parameter at each temperature and Q_i is the result at each specific measurement. The reproducibility is higher than 99% for both the thermometers (Figure 3e).

The emission in the second biological window at about 1060 nm ($^4F_{3/2} \rightarrow {}^4I_{11/2}$ transition) can also be used to design a NIR-to-NIR luminescent thermometer based on the Kramers doublets of $^4F_{3/2}$ with a linearity in the 240−600 K range and a $\Delta E_Z = 135 \pm 3\ cm^{-1}$ estimated from the fit (Figure S3). Also in this case, the thermometric parameters are quite promising, in agreement with the literature and with a high reproducibility.

It is interesting to note that these results suggest a strong potential of the β-Bi_2O_3:Y^{3+},Nd^{3+} system also in the field of anti-counterfeiting. Indeed, the optical security tags conventionally proposed are based on luminescent species (molecules or phosphors) storing a code linked to a specific spectrum, while the encoding system consists of specific luminescent emission patterns achieved by multi-tags for a higher capability.[4] Therefore, combining the NIR-to-NIR strategy for Nd^{3+} with the impossibility to excite the system in the UV/blue spectral range together with the Boltzmann-based thermometric performance and the colorimetric/thermochromic properties of the phosphor, it is possible to use the material as a tag with an extremely high encoding capacity.

Multimodal Thermometric Strategy: Exploiting the Temperature-Dependent Narrow Band gap Edge, f−f Transitions, and Colorimetric Parameters. Luminescence can be strongly quenched by many non-radiative processes influencing the reliability of the read-out temperature of the conventional LIR-based thermometers. In this view, the use of absorption (reflectance) instead of the luminescence could broaden the possibility to develop new families of thermometers with suitable performance and high reliability for specific applications.

With the aim of investigating this potential alternative strategy for temperature sensing, the temperature dependence of the reflectance spectra was investigated in the 300−640 K range (Figure 4a). A clear effect of the temperature on the host is evidenced by the change of the reflectance (absorption) edge with the band gap variation (Figure 4a,b). By considering the extrapolation of the optical band gap energy previously reported with the use of the Tauc plot of the Kubelka−Munk function for a direct band gap semiconductor (Figure 4c), the temperature dependence of the band gap energy was evaluated. As shown in Figure 4d, the decrease of the band gap energy with temperature can be fitted, resulting in a linear trend with a slope of $(-6.2 \pm 0.1)\cdot10^{-4}$ eV/K. This behavior could be used as a thermal sensor, but from the application point of view, the automatic calculation of the E_g has some drawback. Instead, the value of reflectance at 650 nm can be used to follow the effect in a simpler way. In addition, to develop a ratiometric thermometer based on the reflectance spectra, the absorption due to the $^4F_{5/2}$ + $^2H_{9/2}$ is used. Therefore, we introduce the reflectance intensity ratio (RIR) between the reflectance at 650 and 810 nm as the thermal parameter

$$\mathrm{RIR} = \frac{R_{650}}{R_{810}}$$

where R_{650} and R_{810} are the reflectance intensities at 650 and 810 nm, respectively.

The temperature dependence of the RIR is shown in Figure 4e along with the absolute and relative sensitivities estimated. The trend of the relative sensitivity shows a maximum of 0.21% K^{-1} at 550 K. Even though the values are not particularly high, it is important to underline that f−f transitions are only affected to a small extent by temperature in terms of the emission line position with a small error in the identification. Therefore, the use of the reflectance at 650 and 810 nm characterizes the band-to-band transition of the β-Bi_2O_3 and the Nd^{3+} absorption band, respectively (Figure 4f), with a consequent reliable thermometer based on reflectance measurements.

With the idea to develop an automatic analysis during the acquisition, the colorimetric parameters a^* and b^* of the CIELAB color space (CIE 1976 $L^*a^*b^*$[61]) can be alternatively used. The a^*-axis represents approximately the amount of red (positive) or green (negative), while the b^*-axis is approximately the amount of yellow (positive) or blue (negative). Figure 4g shows the colorimetric parameters a^* and b^* as a function of the temperature.

The calculation of such parameters is conventionally implemented in most of the software commonly used in the lab, and they can be easily and automatically measured. The simple ratio between a^* and b^* is proposed as the thermometric parameter $Q = a^*/b^*$ reflecting the effect of temperature on β-Bi_2O_3:Y^{3+},Nd^{3+} in terms of color (Figure 4h). Moreover, an additional promising colorimetric parameter of the CIELAB space suitable for temperature sensing (Figure 4i) is the hue angle h_{ab}, defined as:

$$h_{ab} = \arctan(b^*/a^*)$$

The study of this parameter gives not only interesting values of relative sensitivity obtained at high temperatures ($2\%\cdot K^{-1}$ at 650 K) but also promising values of absolute sensitivity (Figure 4j,k). The S_a values for the thermometer based on the hue angle h_{ab} are higher than $5\cdot10^{-2}$ K^{-1} in the whole temperature range explored. This is particularly important considering the inverse proportionality between S_a and the thermal resolution.[62−64] The hue angle is demonstrated to be particularly promising also with respect to other the common colorimetric parameters calculated in the CIELAB color space (see the results for the chroma C^*_{ab} and the color difference ΔE^*_{ab} in the Supporting Information, Figure S4).

It is worth mentioning that this strategy is particularly interesting in terms of reliability and easy accessibility, being already implemented in common software. Therefore, depending on the temperature range of interest for the specific application, this multimodal system allows the selection of the most suitable thermal sensing mode between the conventional LIR-based technique and the RIR/colorimetric techniques based on the thermochromic behavior of the material.

CONCLUSIONS

In summary, we demonstrate the potential of the Y-stabilized β-Bi_2O_3:Nd^{3+} system as a prototype of lanthanide-doped narrow band gap materials for optical multimodal thermometry in which (i) the Nd^{3+} luminescence can be used to design

https://doi.org/10.1021/acs.chemmater.2c01262
Chem. Mater. 2022, 34, 8198−8206

NIR-to-NIR Boltzmann-based luminescent thermometers and (ii) a fundamental property of the host, such as the temperature dependence of the band gap edge (and corresponding colorimetric parameters) tuning, can be used to design reliable thermometric parameters to be probed by simple reflectance measurements.

The results of the conventional Boltzmann-based luminescence thermometers show interesting performances, in agreement with the literature. In situ analysis of the temperature dependence of the reflectance spectra demonstrates how, being an intrinsic property of the material, the temperature dependence of the band gap shifts along with the Nd^{3+} absorptions can be easily used to design a reliable thermometer. Moreover, among the common colorimetric parameters calculated in the CIELAB color space, the hue angle h_{ab} is demonstrated to be particularly promising in terms of relative sensitivity and reliability with an additional advantage of easy accessibility, being already implemented in software used in the worldwide laboratories. In this context, the approach paves the way for the design of a class of luminescent/thermochromic thermometers exploiting the simple experimental setup, and the performance of the prototype used to propose this approach could be improved by employing materials with larger band gap energy variations with temperature such as in the case of metal halide perovskites.

EXPERIMENTAL SECTION

Chemical Reagents and Synthesis. $(Bi_{0.945}Y_{0.05}Nd_{0.005})_2O_3$ sample (labeled as β-Bi_2O_3:Y^{3+},Nd^{3+}) was prepared by the solid-state reaction method. The chemical reagents Bi_2O_3 (99.99%), Y_2O_3 (99.99%), and Nd_2O_3 (99.99%) were used as starting materials, grounded in an alumina mortar to form a homogeneous fine powder mixture, and pressed into a pellet with a uniaxial loading of 50 MPa in a stainless steel molt. The pellet was fired at 780 °C for 6 h in an air atmosphere.

Materials Characterization. XRPD patterns were recorded at RT by means of a Philips diffractometer with a PW 1319 goniometer with Bragg−Brentano geometry equipped with Cu Kα radiation (λ = 1.54056 Å), a focusing graphite monochromator on the diffracted beam and with a proportional counter with an electronic pulse height discrimination. In order to improve the signal-to-noise ratio to perform Rietveld refinement, the data were collected with a step size of 0.05° in the preset-time mode (10 s) and at least three runs were measured.

The diffuse reflectance spectra were collected by a spectrophotometer (UV3600, Shimadzu) equipped with an integrating sphere and barium sulfate was used as standard. The in situ temperature dependence diffuse reflectance experiments were performed by means of a quadrifurcated 600 mm-core Low-OH-Silica reflectance fiber optic probe coupled with a CCD spectrometer blazed at 500 nm (QE-65Pro, Ocean Optics) and a tungsten halogen lamp (LS-1, Ocean Optics) as the light source.

Photoluminescence (PL) measurements were performed under excitation by means of a 745 nm laser (MDL-III-745-30 mW, Changchun New Industries Optoelectronics Tech. Co. Ltd.), and spectra were recorded with a Si CCD spectrometer (QE-65Pro, Ocean Optics) and an InGaAs-based spectrometer (NIRQuest512, Ocean Optics) for the NIR region, coupled to a double fiber. The PL excitation (PLE) spectrum was recorded by an InGaAs photodiode (IGA-030-H, Electro-Optical System Inc.) coupled with a short-cut (990 nm) and a longcut (1300 nm) filter, a monochromator (SpectraPro-300i, Acton Research Corporation) to tune the excitation wavelengths, and a 100 W halogen lamp (MHAA-100W, Moritex Corporation) as the excitation source. Time-resolved photoluminescence measurements were carried out at room temperature by exciting with a 590 nm pulsed LED (SpectraLED, Thorlabs) in a Horiba-Jobin Yvon Fluorolog 3 spectrofluorometer. The detection system consists of an iHR300 single grating monochromator coupled to a liquid N_2-cooled R5509-73 Hamamatsu PMT operating in the IR region.

The temperature dependence of PL spectra and reflectance spectra were investigated with a temperature-controlled stage (10035 L, Linkam). The PL and PLE spectra were calibrated by means of a standard halogen lamp (DH-2000CAL, Ocean Optics) to obtain spectra on the photon flux scale and converted to photon flux per energy interval using the Jacobian transformation.

First-Principles Calculations. DFT calculations were performed using the plane wave pseudopotential technique implemented in the CASTEP module of the Materials Studio 2021 package to obtain the density of states (DOSs) of β-Bi_2O_3. The ionic core electrons were replaced by the on-the-fly ultrasoft pseudopotentials. The generalized gradient approximation with Perdew-Berke-Ernzerhof for solids (PBEsol) is used as the exchange−correlation energy term. Relativistic effects are taken into account at the level of the Koelling−Harmon approximation of the Dirac equation. The plane-wave basis cutoff energy and k-point grids were chosen as 630 eV and 2 × 2 × 3, respectively.

ASSOCIATED CONTENT

Supporting Information

The Supporting Information is available free of charge at https://pubs.acs.org/doi/10.1021/acs.chemmater.2c01262.

Parameters obtained from the Rietveld refinement analysis, PL decay curve of the material, absolute sensitivity versus relative sensitivity plot and data for a series of Nd^{3+}-activated Boltzmann thermometers, NIR-to-NIR Boltzmann thermometry in the second biological window (temperature dependence of PL spectra, Boltzmann plot, absolute sensitivity, relative sensitivity, and repeatability), thermometric parameters and performances based on chroma C^*_{ab} and the color difference ΔE^*_{ab}, and colorimetric parameter values at different temperatures (PDF)

AUTHOR INFORMATION

Corresponding Authors

Michele Back − *Graduate School of Human and Environmental Studies, Kyoto University, Kyoto 606-8501, Japan; Department of Molecular Sciences and Nanosystems, Ca' Foscari University of Venice, Venice-Mestre 30170, Italy;* orcid.org/0000-0003-1121-9414; Email: michele.back@unive.it

Setsuhisa Tanabe − *Graduate School of Human and Environmental Studies, Kyoto University, Kyoto 606-8501, Japan;* orcid.org/0000-0002-7620-0119; Email: tanabe.setsuhisa.4v@kyoto-u.ac.jp

Authors

Jian Xu − *Graduate School of Human and Environmental Studies, Kyoto University, Kyoto 606-8501, Japan; International Center for Young Scientists (ICYS), National Institute for Materials Science (NIMS), Tsukuba 305-0044 Ibaraki, Japan;* orcid.org/0000-0002-1040-5090

Jumpei Ueda − *Graduate School of Human and Environmental Studies, Kyoto University, Kyoto 606-8501, Japan;* Present Address: Materials Chemistry Frontiers, Japan Advanced Institute of Science and Technology (JAIST), 1−1, Asahidai, Nomi, Ishikawa 923-1292, Japan; orcid.org/0000-0002-7013-9708

https://doi.org/10.1021/acs.chemmater.2c01262
Chem. Mater. 2022, 34, 8198−8206

Alvise Benedetti − *Department of Molecular Sciences and Nanosystems, Ca' Foscari University of Venice, Venice-Mestre 30170, Italy*

Complete contact information is available at: https://pubs.acs.org/10.1021/acs.chemmater.2c01262

Author Contributions

The manuscript was written through contributions of all authors. All authors have given approval to the final version of the manuscript.

Notes

The authors declare no competing financial interest.

■ ACKNOWLEDGMENTS

The work by M.B. was financially supported by the Grant-In-Aid for JSPS Fellows (Grant no. 17F17761). This work was supported by the Grant-in-Aid for Scientific Research B (Grant no. 19H02798).

■ REFERENCES

(1) Geusic, J. E.; Marcos, H. M.; Van Uitert, L. G. Laser oscillations in Nd-doped yttrium aluminium, yttrium gallium and gadolinium garnets. *Appl. Phys. Lett.* **1964**, *4*, 182.

(2) Eliseeva, S. V.; Bünzli, J.-C. G. Lanthanide luminescence for functional materials and bio-sciences. *Chem. Soc. Rev.* **2010**, *39*, 189−227.

(3) Jaque, D.; Richard, C.; Viana, B.; Soga, K.; Liu, X.; García Solé, J. Inorganic nanoparticles for optical bioimaging. *Adv. Opt Photon* **2016**, *8*, 1−103.

(4) Arppe, R.; Sørensen, T. J. Physical unclonable functions generated through chemical methods for anti-counterfeiting. *Nat. Rev. Chem.* **2017**, *1*, 0031.

(5) Brites, C. D.; Balabhadra, S.; Carlos, L. D. Lanthanide-based thermometers: At the cutting-edge of luminescence thermometry. *Adv. Opt. Mater.* **2018**, *7*, 1801239.

(6) Dramićanin, M. D. Trends in luminescence thermometry. *J. Appl. Phys.* **2020**, *128*, 040902.

(7) Runowski, M.; Woźny, P.; Martín, I. R. Optical pressure sensing in vacuum and high-pressure ranges using lanthanide-based luminescent thermometer-manometer. *J. Mater. Chem. C* **2021**, *9*, 4643−4651.

(8) Back, M.; Trave, E.; Mazzucco, N.; Riello, P.; Benedetti, A. Tuning the upconversion light emission by bandgap engineering in bismuth oxide-based upconverting nanoparticles. *Nanoscale* **2017**, *9*, 6353−6361.

(9) Back, M.; Trave, E.; Riello, P.; Joos, J. J. Insight into the upconversion luminescence of highly efficient lanthanide-doped Bi_2O_3 nanoparticles. *J. Phys. Chem. C* **2018**, *122*, 7389−7398.

(10) Riente, P.; Matas Adams, A. M.; Albero, J.; Palomares, E.; Pericàs, M. A. Light-driven organocatalysis using inexpensive, nontoxic Bi_2O_3 as the photocatalyst. *Angew. Chem., Int. Ed.* **2014**, *53*, 9613−9616.

(11) Li, J.; Yu, Y.; Zhang, L. Bismuth oxyhalide nanomaterials: layered structures meet photocatalysis. *Nanoscale* **2014**, *6*, 8473−8488.

(12) Choi, W. S.; Chisholm, M. F.; Singh, D. J.; Choi, T.; Jellison, G. E.; Lee, H. N. Wide bandgap tunability in complex transition metal oxides by site-specific substitution. *Nat. Commun.* **2012**, *3*, 689.

(13) Nechache, R.; Harnagea, C.; Li, S.; Cardenas, L.; Huang, W.; Chakrabartty, J.; Rosei, F. Bandgap tuning of multiferroic oxide solar cells. *Nat. Photonics* **2015**, *9*, 61−67.

(14) Park, B. H.; Kang, B. S.; Bu, S. D.; Noh, T. W.; Lee, J.; Jo, W. Lanthanum-substituted bismuth titanate for use in non-volatile memories. *Nature* **1999**, *401*, 682−684.

(15) Weber, M. J.; Monchamp, R. R. Luminescence of $Bi_4Ge_3O_{12}$: Spectral and decay properties. *J. Appl. Phys.* **1973**, *44*, 5495.

(16) Rasche, B.; Isaeva, A.; Ruck, M.; Borisenko, S.; Zabolotnyy, V.; Büchner, B.; Koepernik, K.; Ortix, C.; Richter, M.; van den Brink, J. Stacked topological insulator built from bismuth-based graphene sheet analogues. *Nat. Mater.* **2013**, *12*, 422−425.

(17) Autès, G.; Isaeva, A. L.; Moreschini, J. C.; Johannsen, A.; Pisoni, R.; Mori, W.; Zhang, T. G.; Filatova, A. N.; Kuznetsov, L.; Forró, W.; Van den Broek, Y.; Kim, K. S.; et al. A novel quasi-one-dimensional topological insulator in bismuth iodide β-Bi_4I_4. *Nat. Mater.* **2016**, *15*, 154−158.

(18) Zaccariello, G.; Back, M.; Zanello, M.; Canton, P.; Cattaruzza, E.; Riello, P.; Alimonti, A.; Benedetti, A. Formation and controlled growth of bismuth titanate phases into mesoporous silica nanoparticles: An efficient self-sealing nanosystem for UV filtering in cosmetic formulation. *ACS Appl. Mater. Interfaces* **2017**, *9*, 1913−1921.

(19) Zaccariello, G. M.; Back, A.; Benedetti, P.; Canton, E.; Cattaruzza, H.; Onoda, A.; Glisenti, A.; Alimonti, B.; Bocca, P.; Riello, P. Bismuth titanate-based UV filters embedded mesoporous silica nanoparticles: Role of bismuth concentration in the self-sealing process. *J. Colloid Interface Sci.* **2019**, *549*, 1−8.

(20) Chen, A.; Zhou, H.; Bi, Z.; Zhu, Y.; Luo, Z.; Bayraktaroglu, A.; Phillips, J.; Choi, E.-M.; MacManus-Discoll, J. L.; Pennycook, S. J.; et al. A new class of room-temperature multiferroic thin films with bismuth-based supercell structure. *Adv. Mater.* **2013**, *25*, 1028−1032.

(21) Huang, H.; Wang, Z.; Huang, B.; Wang, P.; Zhang, X.; Qin, X.; Dai, Y.; Zhou, G.; Whangbo, M.-H. Intense single red emission induced by near-infrared irradiation using a narrow bandgap oxide $BiVO_4$ as the host for Yb^{3+} and Tm^{3+} ions. *Adv. Opt. Mater.* **2018**, *6*, 1701331.

(22) Okabe, K.; Inada, N.; Gota, C.; Harada, Y.; Funatsu, T.; Uchiyama, S. Intracellular temperature mapping with a fluorescent polymeric thermometer and fluorescence lifetime imaging microscopy. *Nat. Commun.* **2012**, *3*, 705.

(23) Piñol, R.; Zeler, J.; Brites, C. D. S.; Gu, Y.; Téllez, P.; Carneiro Neto, A. N.; da Silva, T. E.; Moreno-Loshuertos, R.; Fernandez-Silva, P.; Gallego, A. I.; Martinez-Lostao, L.; Martínez, A.; Carlos, L. D.; Millán, A. Real-time intracellular temperature imaging using lanthanide-bearing polymeric micelles. *Nano Lett.* **2020**, *20*, 6466−6472.

(24) Bednarkiewicz, A.; Drabik, J.; Trejgis, K.; Jaque, D.; Ximendes, E.; Marciniak, L. Luminescence based temperature bio-imaging: Status, challenges, and perspectives. *Appl. Phys. Rev.* **2021**, *8*, 011317.

(25) van Swieten, T. P.; van Omme, T.; van den Heuvel, D. J.; Vonk, S. J. W.; Spruit, R. G.; Meirer, F.; Garza, H. H. P.; Weckhuysen, B. M.; Meijerink, A.; Rabouw, F. T.; Geitenbeek, R. G. Mapping elevated temperatures with a micrometer resolution using the luminescence of chemically stable upconversion nanoparticles. *ACS Appl. Nano Mater.* **2021**, *4*, 4208−4215.

(26) Back, M.; Ueda, J.; Xu, J.; Murata, D.; Brik, M. G.; Tanabe, S. Ratiometric luminescent thermometers with a customized phase-transition-driven fingerprint in perovskite oxides. *ACS Appl. Mater. Interfaces* **2019**, *11*, 38937−38945.

(27) Brites, C. D. S.; Zhuang, B.; Debasu, M. L.; Ding, D.; Qin, X.; Maturi, F. E.; Lim, W. W. Y.; Soh, D. W.; Rocha, J.; Yi, Z.; Liu, X.; Carlos, L. D. Decoding a percolation phase transition of water at ∼330 K with a nanoparticle ruler. *J. Phys. Chem. Lett.* **2020**, *11*, 6704−6711.

(28) Geitenbeek, R. G.; Nieuwelink, A.-E.; Jacobs, T. S.; Salzmann, B. B. V.; Goetze, J.; Meijerink, A.; Weckhuysen, B. M. In situ luminescence thermometry to locally measure temperature gradients during catalytic reactions. *ACS Catal.* **2018**, *8*, 2397−2401.

(29) Ravenhorst, I. K.; Geitenbeek, R. G.; Eerden, M. J.; Tijn van Omme, J. T.; Peréz Garza, H. H. P.; Meirer, F.; Meijerink, A.; Weckhuysen, B. M. In situ local temperature mapping in microscopy nano-reactors with luminescence thermometry. *ChemCatChem* **2019**, *11*, 5505−5512.

(30) Hartman, T.; Geitenbeek, R. G.; Whiting, G. T.; Weckhuysen, B. M. Operando monitoring of temperature and active species at the single catalyst particle level. *Nat. Catal.* **2019**, *2*, 986−996.

(31) Back, M.; Ueda, J.; Nambu, H.; Fujita, M.; Yamamoto, A.; Yoshida, H.; Tanaka, H.; Brik, M. G.; Tanabe, S. Boltzmann thermometry in Cr^{3+}-doped Ga_2O_3 polymorphs: The structure matters. *Adv. Opt. Mater.* **2021**, *9*, 2100033.
(32) Marciniak, L.; Bednarkiewicz, A.; Stefanski, M.; Tomala, R.; Hreniak, D.; Strek, W. Near infrared absorbing near infrared emitting highly-sensitive luminescent nanothermometer based on Nd^{3+} to Yb^{3+} energy transfer. *Phys. Chem. Chem. Phys.* **2015**, *17*, 24315−24321.
(33) Marciniak, L.; Bednarkiewicz, A.; Drabik, J.; Trejgis, K.; Strek, W. Optimization of highly sensitive YAG:Cr^{3+},Nd^{3+} nanocrystal-based luminescent thermometer operating in an optical window of biological tissues. *Phys. Chem. Chem. Phys.* **2017**, *19*, 7343−7351.
(34) Gao, Y.; Huang, F.; Lin, H.; Zhou, J.; Xu, J.; Wang, Y. A novel optical thermometry strategy based on diverse thermal response from two intervalence charge transfer states. *Adv. Funct. Mater.* **2016**, *26*, 3139−3145.
(35) Souza, A. S.; Nunes, L. A. O.; Silva, I. G. N.; Oliveira, F. A. M.; da Luz, L. L.; Brito, H. F.; Felinto, M. C. F. C.; Ferreira, R. A. S.; Júnior, S. A.; Carlos, L. D.; Malta, O. L. Highly-sensitive Eu^{3+} ratiometric thermometers based on excited state absorption with predictable calibration. *Nanoscale* **2016**, *8*, 5327−5333.
(36) Trejgis, K.; Bednarkiewicz, A.; Marciniak, L. Engineering excited state absorption based nanothermometry for temperature sensing and imaging. *Nanoscale* **2020**, *12*, 4667−4675.
(37) McLaurin, E. J.; Bradshaw, L. R.; Gamelin, D. R. Dual-emitting nanoscale temperature sensors. *Chem. Mater.* **2013**, *25*, 1283−1292.
(38) Back, M.; Trave, E.; Ueda, J.; Tanabe, S. Ratiometric optical thermometer based on dual near-infrared emission in Cr^{3+}-doped bismuth-based gallate host. *Chem. Mater.* **2016**, *28*, 8347−8356.
(39) Casagrande, E.; Back, M.; Cristofori, D.; Ueda, J.; Tanabe, S.; Palazzolo, S.; Rizzolio, F.; Canzonieri, V.; Trave, E.; Riello, P. Upconversion-mediated Boltzmann thermometry in double-layered Bi_2SiO_5:Yb^{3+},Tm^{3+}@SiO_2 hollow nanoparticles sensors. *J. Mater. Chem. C* **2020**, *8*, 7828−7836.
(40) Suta, M.; Meijerink, A. A theoretical framework for ratiometric single ion luminescent thermometers—Thermodynamic and kinetic guidelines for optimized performance. *Adv. Theory Simul.* **2020**, *3*, 2000176.
(41) Yu, D.; Li, H.; Zhang, D.; Zhang, Q.; Meijerink, A.; Suta, M. One ion to catch them all: Targeted high-precision Boltzmann thermometry over a wide temperature range with Gd^{3+}. *Light Sci. Appl.* **2021**, *10*, 236.
(42) Sammes, N. M.; Tompsett, G. A.; Näfe, H.; Aldinger, F. Bismuth based oxide electrolytes - Sructure and ionic conductivity. *J. Eur. Ceram. Soc.* **1999**, *19*, 1801−1826.
(43) Drache, M.; Roussel, P.; Wignacourt, J.-P. Structures of oxide mobility in Bi-Ln-O materials: Heritage of Bi_2O_3. *Chem. Rev.* **2007**, *107*, 80−96.
(44) Malavasi, L. C. A. J.; Fisher, M. S.; Islam, M. S. Oxide-ion proton conducting electrolyte materials for clean energy applications: structural and mechanistic features. *Chem. Soc. Rev.* **2010**, *39*, 4370−4387.
(45) Walsh, A.; Watson, G. W.; Payne, D. J.; Edgell, R. G.; Guo, J.; Glans, P. A.; Learmonth, T.; Smith, K. E. Electronic structure of the α and δ phase of Bi_2O_3: A combined ab initio and x-ray spectroscopy study. *Phys. Rev. B: Condens. Matter Mater. Phys.* **2006**, *73*, 235104.
(46) Walsh, A.; Watson, G. W. Polymorphism in Bismuth Stannate: A First-Principles Study. *Chem. Mater.* **2007**, *19*, 5158−5164.
(47) Tauc, J.; Grigorovici, R.; Vancu, A. Optical properties and electronic structure of amorphous germanium. *Phys. Status Solidi B* **1966**, *15*, 627−637.
(48) Kubelka, P.; Munk, F. Ein Beitrag Zur Optik Der Farbanstriche. *Z. Tech. Phys.* **1931**, *12*, 593−601.
(49) Cheng, H.; Huang, B.; Lu, J.; Wang, Z.; Xu, B.; Qin, X.; Zhang, X.; Dai, Y. Synergistic effect of crystal and electronic structures on the visible-light-driven photocatalytic performances of Bi_2O_3 polymorphs. *Phys. Chem. Chem. Phys.* **2010**, *12*, 15468−15475.
(50) Lu, Y.; Zhao, J.; Zhao, Y.; Song, Z.; Huang, F.; Gao, N.; Li, Y.; Li, Y. Induced aqueous synthesis of metastable β-Bi_2O_3 microcrystals for visible-light photocatalyst study. *Cryst. Growth Des.* **2015**, *15*, 1031−1042.
(51) Dorenbos, P. Determining binding energies of valence-band electrons in insulators and semiconductors via lanthanide spectroscopy. *Phys. Rev. B: Condens. Matter Mater. Phys.* **2013**, *87*, 035118.
(52) Dorenbos, P. Electronic structure of Bi-activated luminescent compounds and pure bismuth photocatalytic compounds. *ECS J. Solid State Sci. Technol.* **2021**, *10*, 086002.
(53) Back, M.; Ueda, J.; Ambrosi, E.; Cassandro, L.; Cristofori, D.; Ottini, R.; Riello, P.; Sponchia, G.; Asami, K.; Tanabe, S.; Trave, E. Lanthanide-doped bismuth-based fluoride nanocrystalline particles: Formation, spectroscopic investigation, and chemical stability. *Chem. Mater.* **2019**, *31*, 8504−8514.
(54) Hou, J.; Yang, C.; Wang, Z.; Zhou, W.; Jiao, S.; Zhu, H. In situ synthesis of α-β phase heterojunction on Bi_2O_3 nanowires with exceptional visible-light photocatalytic performance. *Appl. Catal.* **2013**, *142-143*, 504−511.
(55) Gandhi, A. C.; Lai, C.-Y.; Wu, K.-T.; Ramacharyulu, P. V. R. K.; Koli, V. B.; Cheng, C.-L.; Ke, S.-C.; Wu, S.-Y. Phase transformation and room temperature stabilization of various Bi_2O_3 nanopolymorphs: effect of oxygen-vacancy defects and reduced surface energy due to adsorbed carbon species. *Nanoscale* **2020**, *12*, 24119−24137.
(56) Hemmer, E.; Benayas, A.; Légaré, F.; Vetrone, F. Exploiting the biological windows: Current perspectives on fluorescent bioprobes emitting above 1000 nm. *Nanoscale* **2016**, *1*, 168−184.
(57) Benayas, A.; del Rosal, B.; Pérez-Delgado, A.; Santacruz-Gómez, K.; Jaque, D.; Hirata, G. A.; Vetrone, F. Nd YAG near-infrared luminescent nanothermometers. *Adv. Opt. Mater.* **2015**, *3*, 687−694.
(58) Skripka, A.; Morinvil, A.; Matulionyte, M.; Cheng, T.; Vetrone, F. Advancing neodymium single-band nanothermometry. *Nanoscale* **2019**, *11*, 11322−11330.
(59) Suta, M.; Antić, Z.; Đorđević, V.; Kuzman, S.; Dramićanin, M. D.; Meijerink, A. Making Nd^{3+} a sensitive luminescent thermometer for physiological temperatures − An account of pitfalls in Boltzmann thermometry. *Nanomaterials* **2020**, *10*, 543.
(60) Back, M.; Casagrande, E.; Trave, E.; Cristofori, D.; Ambrosi, E.; Dallo, F.; Roman, M.; Ueda, J.; Xu, J.; Tanabe, S.; Benedetti, A.; Riello, P. Confined-melting-assisted synthesis of bismuth silicate glass-ceramic nanoparticles: Formation and optical thermometry investigation. *ACS Appl. Mater. Interfaces* **2020**, *12*, 55195−55204.
(61) Witt, K. Understanding the CIE System. In *Colorimetry*; Schanda, J. C., Ed.; Wiley, 2007; Vol. *4*.
(62) Quintanilla, M.; Liz-Marzán, L. Guiding rules for selecting a nanothermometer. *Nano Today* **2018**, *19*, 126−145.
(63) Back, M.; Ueda, J.; Brik, M. G.; Lesniewski, T.; Grinberg, M.; Tanabe, S. Revisiting Cr^{3+}-doped $Bi_2Ga_4O_9$ spectroscopy: Crystal field effect and optical thermometric behavior of near-infrared-emitting singly-activated phosphors. *ACS Appl. Mater. Interfaces* **2018**, *10*, 41512−41524.
(64) Back, M.; Ueda, J.; Xu, J.; Asami, K.; Brik, M. G.; Tanabe, S. Effective ratiometric luminescent thermal sensor by Cr^{3+}-doped mullite $Bi_2Al_4O_9$ with robust and reliable performances. *Ad. Opt. Mater.* **2020**, *8*, 2000124.

https://doi.org/10.1021/acs.chemmater.2c01262
Chem. Mater. 2022, 34, 8198−8206